Noname manuscript No.
(will be inserted by the editor)

CRSM: a practical crowdsourcing-based road surface monitoring system

Kongyang Chen · Guang Tan · Mingming Lu · Jie Wu

Received: date / Accepted: date

Abstract Detecting road potholes and road roughness levels is key to road condition monitoring, which impacts transport safety and driving comfort. We propose a crowdsourcing-based road surface monitoring system, simply called *CRSM*. CRSM can effectively detect road potholes and evaluate road roughness levels using hardware modules mounted on distributed vehicles. These modules use low-end accelerometers and GPS devices to obtain vibration patterns, locations, and vehicle velocities. Considering the high cost of onboard storage and wireless transmission, a novel light-weight data mining algorithm is proposed to detect road surface events and transmit potential pothole information to a central server. The server gathers reports from multiple vehicles, and makes a comprehensive evaluation on road surface quality. We have implemented a product-quality system, and have deployed it on 100 taxies in the Shenzhen urban area. The results show that CRSM can detect road potholes with 90% accuracy, with nearly zero false alarms. CRSM can also evaluate road roughness levels correctly, even with some interferences from small bumps or potholes.

Keywords Road surface monitoring · Pothole detection · Gaussian Mixture Model · Road surface roughness

K. Chen
Shenzhen Institutes of Advanced Technology, Chinese Academy of Sciences, Shenzhen 518055, China
Shenzhen College of Advanced Technology, University of Chinese Academy of Sciences, Shenzhen 518055, China
E-mail: ky.chen@siat.ac.cn

G. Tan
Shenzhen Institutes of Advanced Technology, Chinese Academy of Sciences, Shenzhen 518055, China

M. Lu
Central South University, Changsha 410083, China

J. Wu
Temple University, PA 19122, USA

1 Introduction

Road surface conditions have been a public concern in modern society. City municipalities have paid millions of dollars to detect, maintain, and repair the roadways each year. A study by the U.S. Department of Transportation has shown that road conditions are an essential factor of highway quality [3]. One of the main road surface condition metrics is the density of road potholes, which can cause serious damage, and should be repaired as early as possible. In addition, the roughness level of road surfaces is also an important metric that reflects the condition of road health. This paper seeks to evaluate these two metrics in an efficient way, following a crowdsourcing approach.

Our basic observation is that accelerometers will experience significant vibration when the vehicle is passing an "abnormal" section of road (e.g., potholes, manholes, and expansion joints), thus producing abnormal readings compared to data from smooth road surfaces. We only store and transmit data associated with these abnormal events to a central server. Meanwhile, we try to establish a relationship between the road surface roughness level and acceleration signal. According to the Technical Code of Maintenance for Urban Road CJJ36-2006 [25], one of the industry standards in China, we provide a low-cost solution for road roughness detection.

We describe the design and implementation of a crowdsourcing-based road surface monitoring system, simply called *CRSM*. It can detect road potholes and evaluate road roughness levels with our hardware modules installed on distributed vehicles, which are wirelessly connected to a central server. A CRSM module consists of an accelerometer and a GPS module to identify road vibration and obtain location and vehicle velocity. To minimize storage and transmission costs, a light-weight data mining algorithm, namely *i-GMM* (improved Gaussian Mixture Model), is proposed to detect road surface events, and transmit pothole information to the server. CRSM also presents a road roughness classification algorithm to determine the road roughness level. Experimental results show that CRSM can detect road potholes with 90% accuracy, with nearly zero false alarms. CRSM can also evaluate road roughness levels correctly, even with some interferences from small bumps or potholes.

The highlight of CRSM is its practicality. The system has been deployed on 100 taxies in the Shenzhen urban area, and has operated for more than two years, providing useful information for the Transportation Bureau of Shenzhen Municipal Government. The system has also been tested in the Highway Traffic Testing Field of Ministry of Transportation in Beijing. CRSM makes the following contributions to the community of vehicular networking and services:

- An architecture of a crowdsourcing-based road surface monitoring system for both pothole detection and road surface roughness evaluation;
- Algorithms for event detection and pothole identification, improving on previous techniques;
- An online algorithm for road surface roughness evaluation in compliance with industry standards;
- A comprehensive evaluation of the system that brings us lessons on the design of related services and systems.

The remainder of this paper is organized as follows. Section 2 provides a brief overview of previous works. Section 3 gives an overview of our system architecture. Section 4 and Section 5 discuss the methods of road pothole detection and road roughness level classification, respectively. Section 6 presents our evaluation on real taxies. Section 7 discusses future work. Finally, Section 8 concludes this paper.

2 Related work

In this section, we give a brief review of related work on pothole detection and road roughness level classification.

2.1 Road pothole detection

Many road pothole detection solutions have been proposed in this literature. In [1], citizens are encouraged to share and upload the pothole information to public online websites. Various sensors such as 3D laser scanning devices, along with 3D reconstruction algorithms, are used to measure the size of road potholes [11, 12, 14]. They capture the 3D digital models of road surface with a real-time laser scanner, and apply the stereovision technique to extract potholes. In [7,27], cameras are installed on vehicles to record road videos, from which road conditions are inferred with three layer feed forward neural networks. These pothole detection techniques are not convenient enough for deployment, or are too expensive for wide adoption.

Recently, accelerometers have been increasingly utilized in road condition monitoring. Normally, a vehicle vibrates more than normal when passing potholes, contraction joints, manholes, expansion joints, etc. The vibration can be effectively captured by an onboard accelerometer. Given an accelerometer and a GPS device, we can identify a road vibration situation and its corresponding location [26]. This method needs to sense, store, and upload all the acceleration and GPS data to a central server for further processing, such as Pothole Patrol [10], BusNet [13], Nericell [19]. However, the high demand for data storage and data transmission remains a challenging issue.

2.2 Road roughness level classification

Information of road surface roughness is important for evaluating the health status of roads. Xu et al. [24] present a criterion of road roughness based on power spectral density of vehicle vibration. Semiha et al. [20] study the random vibration characteristics of the quarter car model to describe vehicle vibration. Zhang et al. [28] discuss a roughness measurement system based on a laser range finder. Dyer et al. [9] describe how to estimate an international roughness index from noisy profilograph measurements. Hostettler et al. [4] summarize the current equipment for road condition measurement, composed of accelerometers, distance instruments, graphic displays, or some other instruments. These road condition evaluation systems are highly expensive, costing 8,000 to 220,000 dollars for a single vehicle.

3 Overview

In this section, we first present the system architecture of CRSM along with the corresponding hardware

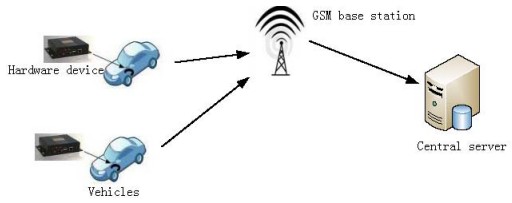

Fig. 1: CRSM system architecture.

design. Then we describe the software architecture of road pothole detection and road roughness level classification.

3.1 System architecture

CRSM uses a set of hardware devices installed on vehicles for data collection and a central server for multi-source data fusion. The system architecture is depicted in Figure 1.

Each onboard hardware module is mainly composed of a microcontroller (MCU), a GPS module, a three-axis accelerometer, and a GSM module. When the vehicle is traveling, the accelerometer reads continuous acceleration data, the GPS module outputs the accurate time, location, and velocity of the vehicle, the MCU executes algorithms to extract useful data, and the GSM module transmits the results to the central server.

More specifically, the onboard module is designed with low-end hardware to facilitate wide adoption in the city. We use a client microprocessor with limited CPU capacity and storage, and a low-end MEMS accelerometer. In detail, the client microprocessor is a 32-bit cortex ARM chip STM32F103 with 72MHz maximum system clock and 256KB memory, which is not sufficient for common algorithm complexity demand and storage demand. The MEMS motion module, LIS33DE, is adopted as the three-axis accelerometer. It has a 100Hz sampling frequency with a 2g dynamic measurement scale. The GPS receiver is the vehicle-mounted HM-CZ02 GPS sensor with 1Hz sampling frequency. Finally, the GSM module is equipped with a common commercial SIM card.

The GSM traffic presents a major cost in the system. In our system, for example, the GSM data budget is no more than 30 MB per month. We therefore cannot transmit the raw data to the central server, as the data is too large in size. Because of this, we transmit only useful information, which is determined by a light weight online data mining algorithm.

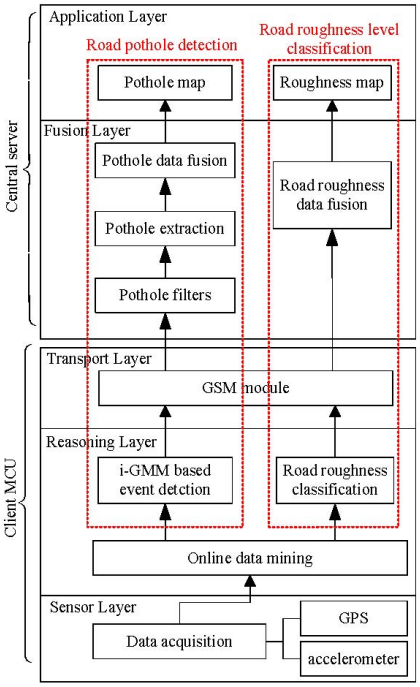

Fig. 2: CRSM software architecture.

3.2 Software architecture

The software architecture of CRSM is presented in Figure 2, which consists of five layers, namely the sensor layer, the reasoning layer, the transport layer, the fusion layer, and the application layer. The bottom three layers are deployed at the client side, where sensor data are acquired, analyzed, and transferred. The top two layers are executed at the server side, where data from multiple sources are fused to generate comprehensive results.

In the sensor layer, raw GPS and accelerometer readings are periodically collected by onboard hardware sensors, which are updated at rates of 1 Hz and 100 Hz, respectively. The sampled data are primarily analyzed by an online data mining method in the reasoning layer. Specifically, an i-GMM-based event detection algorithm is executed to find potential pothole locations, and a road roughness classification algorithm is used to extract road roughness level information. Then, these results are packed and transmitted to the central server by a GSM module in each vehicle.

The central server gathers data from the distributed vehicles, and obtains a comprehensive conclusion in the fusion layer. For road pothole detection, it applies four pothole filters to remove irrelevant events in the received data, employs an EEMD-based pothole extraction method to eliminate interfering events such as decelerating belts, and combines the outcome of multiple

vehicles' pothole detection results. For road roughness detection, road roughness level results are merged with a data fusion method. Finally, a pothole map and a road roughness level map are built to show the global road surface health in the application layer.

4 Road pothole detection

The CRSM system selectively reports useful data to the central server by discarding acceleration data on smooth roads. First, we design an event detection algorithm to identify "abnormal" vibrations. Then the central server will further analyze the data from multiple vehicles to obtain more accurate results.

4.1 Event detection

Event detection is a process for identifying potential potholes on the road surface [21]. An onboard accelerometer can sense vehicle vibrations by examining the z-axis acceleration. Normally, the vibration on abnormal road sections is greater than that on smooth sections, so an abrupt increase of z-axis acceleration often signifies a pothole.

The Z-peak method declares an event if the current z-axis acceleration is larger than a predefined threshold. However, a vehicle's vibration and acceleration vary greatly on different roads, and at different driving velocities. It is therefore impossible to determine a universal threshold that applies to all possible situations.

To address this problem, we introduce a Gaussian Mixture Model (GMM) algorithm for event detection. The GMM can learn the background signal online, without needing to train parameters for different road conditions beforehand; this differs greatly from previous methods. Furthermore, we propose an i-GMM algorithm to overcome the drawbacks of the GMM.

4.2 The Gaussian Mixture Model (GMM)

The z-axis acceleration signal captured from a smooth road may be fitted by a Gaussian distribution. An example of empirical z-axis acceleration is shown in Figure 3, which confirms this hypothesis. The Gaussian distribution with mean μ and variance σ^2:

$$\eta(x|\mu,\sigma^2) = \frac{1}{\sqrt{2\pi}\sigma} e^{-(x-\mu)^2/2\sigma^2}, \tag{1}$$

can be dynamically updated from historic information. In our situation, the magnitude of vibration caused by a pothole is much greater than that caused by a smooth road surface. So a signal X is considered as a pothole if it deviates widely from the mean μ of the smooth road. That is to say, X is a pothole signal if the absolute difference of X and μ is greater than a predefined threshold M_{th} times the standard variance σ, that is

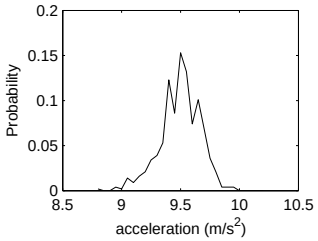

Fig. 3: Distribution of the z-axis acceleration from a smooth road.

$$\left|\frac{X-\mu}{\sigma}\right| > M_{th}. \tag{2}$$

Otherwise, X is considered to be a smooth road signal, and its mean μ and variance σ will be learned as follows:

$$\begin{aligned} \mu' &= (1-\delta)\mu + \delta X \\ \sigma'^2 &= (1-\delta)\sigma^2 + \delta(X-\mu)^2 \\ \delta &= \alpha\eta(X|\mu,\sigma^2), \end{aligned} \tag{3}$$

where α is a learning rate, and δ is α time probability density function learnt from the past signals.

The above method is the single Gaussian model, which is only a rough approximation of the background signal. A better solution with improved accuracy is given by the Gaussian Mixture Model (GMM), which uses K Gaussian distributions to fit the background signals [15, 21], as is evident from the multiple peaks in Figure 3. An intuitive idea is that acceleration signals are generated by various sources and errors which follow their respective Gaussian distributions. So the GMM assigns a weight ω_k to each of the K Gaussian distributions $\omega_k\eta(\mu_k,\sigma_k^2,\omega_k)$ following $\sum_{k=1}^{K}\omega_k = 1$.

Consider a newly sampled signal X. The GMM first updates the parameters of each Gaussian distribution to best fit X, and then estimates X as a background signal or an event.

4.2.1 Online update

If the signal X matches any of the K Gaussian distributions, it means that the current GMM is robust for X. Suppose $\eta(\mu_k,\sigma_k^2,\omega_k)$ is a matched distribution. We add its weight and update its mean and variance as

follows:

$$\begin{aligned}\mu'_k &= (1-\delta)\mu_k + \delta X \\ \sigma'^2_k &= (1-\delta)\sigma^2_k + \delta(X-\mu_k)^2 \\ \omega'_k &= (1-\alpha)\omega_k + \alpha \\ \delta &= \alpha\eta(\mu_k, \sigma^2_k, \omega_k),\end{aligned} \tag{4}$$

In this case, an unmatched distribution holds the same mean and variance, but its weight will be decreased. Its parameters are updated as follows:

$$\begin{aligned}\mu'_k &= \mu_k \\ \sigma'^2_k &= \sigma^2_k \\ \omega'_k &= (1-\alpha)\omega_k.\end{aligned} \tag{5}$$

If the signal X does not match any of the K Gaussian distributions, it shows that the current GMM is not robust for X. The least probable distribution (with the lowest ω_k) is replaced with a new distribution to better fit the current signal X. This new distribution takes on the current signal X as its mean value, with a predefined high variance and a low weight.

$$\begin{aligned}k &= \underset{k}{\operatorname{argmin}}\ \omega_k \\ \mu'_k &= X \\ \sigma'^2_k &= \sigma^2_0 \\ \omega'_k &= \omega_0,\end{aligned} \tag{6}$$

where weights are normalized so that $\sum_{k=1}^{K} \omega'_k = 1$.

4.2.2 Background model estimation

After online update, we would like to determine whether the current signal X is an event. Among the K Gaussian distributions, we are interested in distributions which are most likely to be produced by the background. Intuitively, these distributions have the highest weights and lowest variances. At the same time, the less probable distributions will be downplayed.

Next, the K Gaussian distributions are ordered by ω'_k/σ'_k, so the most likely distributions are placed on top. Then, the top B distributions are selected as the background model,

$$B = \underset{b}{\operatorname{argmin}}(\sum_{k=1}^{b} \omega'_k > T), \tag{7}$$

where T is a predefined threshold to determine how many distributions are used to represent the current background.

Finally, the current signal x is estimated with the B selected distributions. Similar to the single Gaussian model, X is considered as an event if all these B distributions $\eta(\mu'_k, \sigma'^2_k, \omega'_k)$ satisfy

$$M_k = \left|\frac{X-\mu'_k}{\sigma'_k}\right| > M_{th}, \tag{8}$$

where M_{th} is a predefined event detection threshold. Otherwise, X is not considered as an event.

4.3 Two drawbacks of the GMM

When we used the GMM for event detection, we found two drawbacks caused by the variation in velocity.

4.3.1 Drawback 1: fixed event detection threshold

In practice, the vehicle vibration is highly affected by the driving velocity. For example, when driven at a high velocity, the vehicle vibrates greatly and our onboard accelerometer will generate higher vibration amplitude. In fact, Watts et al. [18] have carried out a set of experiments on ground vibration levels with different vehicle velocities, and pointed out that vehicle vibration level and driving velocity are roughly in a linear relationship when velocities are between 15 km/h and 45 km/h. Thus, we can view z-axis accelerations as roughly proportional to vehicle velocities.

Suppose a vehicle moves at a high velocity on a smooth road, causing z-axis acceleration to vary greatly. When we apply the GMM on this smooth road, unmatched distributions keep their means and variances, and matched distributions update their means and variance as follows:

$$\begin{aligned}\mu'_k &= (1-\delta)\mu_k + \delta X \\ \sigma'^2_k &= (1-\delta)\sigma^2_k + \delta(X-\mu_k)^2 \\ \delta &= \alpha\eta(\mu_k, \sigma^2_k, \omega_k),\end{aligned} \tag{9}$$

In our experiments, accelerometers have a 100 Hz sampling rate, so even a short segment of road will generate highly redundant raw data. In this case, we should not set the learning rate α too high, otherwise the GMM keeps little historical information and becomes highly unstable. Generally, we initialize the learning rate α to 0.03. Clearly, the probability density function $\eta(\mu_k, \sigma^2_k, \omega_k)$ is less than 1, and we have $\delta < \alpha$ and $1-\delta \gg \delta$.

When the vehicle is traveling on a smooth road, the mean of Gaussian distribution μ_k is at the same order of magnitude as the current signal X. Hence, we can deduce that $(1-\delta)\mu_k \gg \delta X$ and $\mu'_k \approx (1-\delta)\mu_k$. In other words, the matched distributions decrease their means with a small slope $1-\delta$. For simplicity, we may consider their means as a constant C_1 in a short time

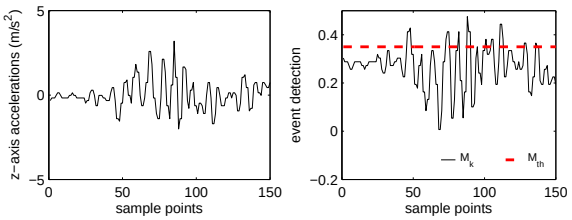

(a) Z-axis acceleration. (b) Event detection with false alarms.

Fig. 4: Event identification at a high velocity.

interval. Similarly, we can conclude that the matched distributions decrease their variance with a small slope $1-\delta$, and can be approximated with a constant C_2 in a short time interval.

According to Equation 8, it follows the event detection expression

$$M_k = \left|\frac{X-\mu'_k}{\sigma'_k}\right| \approx \left|\frac{X-C_1}{C_2}\right|. \tag{10}$$

Here, M_k is roughly linear with the acceleration signal X, and then is approximately proportional to the vehicle velocity V, too.

Suppose the vehicle is traveling at a high velocity, then the GMM event detection expression M_k becomes larger. This causes false alarms when M_k is greater than the fixed threshold M_{th}. Figure 4 shows the z-axis acceleration and event detection expression on a smooth road surface. We see that M_k (solid line in Figure 4(b)) is very similar to the z-axis acceleration (Figure 4(a)). We also observe that M_k is several times greater than the predefined threshold M_{th} (red dashed line in Figure 4(b)), which causes false alarms.

For similar reasons, a low traveling velocity leads to missed events when a fixed event detection threshold is applied.

4.3.2 Drawback 2: fixed learning rate

The GMM uses a fixed learning rate α to update the mean, variance, and weight of each Gaussian distribution, as if the current signal and historical information were equally important. However, this rule no longer applies when the vehicle's velocity changes. For instance, when the vehicle's velocity increases greatly, the z-axis acceleration will also increase, which results in a more significant deviation from historical data. With a fixed learning rate, it will take a longer time to learn and build accurate Gaussian distributions [5].

To deal with this problem, we need to increase the GMM learning rate and bias the learning process toward the current signal. Similarly, we should increase the learning rate when the velocity decreases greatly, while we should use a small learning rate when the vehicle velocity remains almost the same.

In summary, we conclude that a large learning rate is suitable for significant velocity changes, and a small learning rate is suitable for small velocity changes.

4.4 i-GMM

To overcome the GMM's drawbacks, we propose an improved GMM (i-GMM) algorithm to accommodate the variability of velocity.

4.4.1 Event detection threshold

With a fixed event detection threshold, a high velocity will produce more false alarms, and a low velocity will increase missed events. For this reason, the event detection threshold is controlled by a parameter which is roughly linear with the current velocity. The above event detection rule is modified as follows:

The current signal X is considered as an event only if all the B distributions $\eta(\mu'_k, \sigma'^2_k, \omega'_k)$ satisfy

$$M_k = \left|\frac{X-\mu'_k}{\sigma'_k}\right| > M_{th} \cdot \frac{V}{V_{th}}, \tag{11}$$

where V is the current velocity, and V_{th} is a velocity threshold.

4.4.2 Learning rate update

Based on the above discussion, the learning rate is related to the change of velocity. A high learning rate is used for significant velocity changes, and a small learning rate is used for small velocity changes. Hence, the learning rate is considered as a linear function of the velocity changes. The learning rate at the moment t can be adjusted as follows:

$$\begin{aligned} \alpha_t &= \alpha_{min} + (\alpha_{max} - \alpha_{min}) \cdot |\triangle V_t| / V_{tc} \\ \triangle V_t &= \begin{cases} V_t - V_{t-1}, & |V_t - V_{t-1}| <= V_{tc} \\ V_{tc}, & |V_t - V_{t-1}| > V_{tc}, \end{cases} \end{aligned} \tag{12}$$

where α_{min} and α_{max} are the minimum and maximum learning rates; $\triangle V_t$ is the velocity change at time t; V_{tc} is a velocity threshold; V_t and V_{t-1} are velocities at t and $t-1$ moments, respectively. The learning rate is set to the maximum value α_{max}, when the velocity change is greater than a predefined velocity threshold V_{tc}.

4.5 Pothole filters

The CRSM system uses an i-GMM for event detection. Our central server will gather, clean, and fuse event data from the multiple vehicles.

Many disturbance events may be mistaken for road potholes, for example, upon opening or closing the vehicle panels, small bumps, expansion joints, contraction joints, and high velocity vibration. We therefore apply pothole filters to remove anomalous events:

- Velocity filter: it removes events with a zero or very low velocity, for example, when opening or closing the vehicle panels. It rejects events when the velocity is lower than a threshold T_V.
- Z-axis acceleration filter: it removes events with low z-axis acceleration peaks, such as those caused by small bumps. It refuses events whose z-axis acceleration is lower than a threshold T_Z.
- X-z acceleration ratio filter: it deletes events with a small ratio of x-axis acceleration to z-axis acceleration, for example, those caused by expansion joints and contraction joints. It discards events whose x-z acceleration ratio is lower than a threshold T_{XZ}.
- Velocity vs. z-axis acceleration ratio filters: it removes events with a high ratio of velocity to z-axis acceleration, mainly caused by high velocity vibration. It rejects events whose velocity vs. z acceleration ratio is higher than a threshold T_{VZ}.

4.6 Pothole Extraction

Decelerating belts cause vibrations similar to those by potholes. Pothole filters and data fusion cannot effectively distinguish these events. Normally, decelerating belts are longer than potholes in width. This means that a vehicle will pass a pothole on a single side, while it will be pressed on both sides when passing a decelerating belt. Therefore, there are different vibration energy distributions between the tires.

CRSM employs a signal processing algorithm, namely ensemble empirical mode decomposition (EEMD) based pothole extraction algorithm. EEMD deals with the issue of mode mixing and mode splitting by adding white noise to the original signal, which makes it suitable for nonlinear and non-stationary time series analysis [22, 23].

First, decelerating belt and pothole acceleration signals are decomposed with EEMD into several intrinsic mode functions (IMFs):

$$x(t) = \sum_{k=1}^{N} p_k + r_{N+1} \tag{13}$$

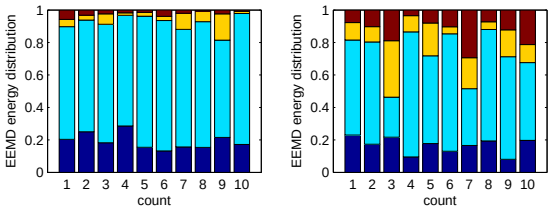

(a) Decelerating belts. (b) Road potholes.

Fig. 5: Four EEMD energy ratios with different events.

where $x(t)$ is the z-axis acceleration; p_k and r_{N+1} are the kth IMF component and the residual error component, respectively; N is the total number of IMFs.

Next, the most significant four EEMD energy components are extracted and normalized with $E_k = P_k^2 / \sum_{k=1}^{N} P_k^2$, where E_k is the k^{th} energy components. Figure 5(a) shows the EEMD energy ratios of the leading four components from ten different decelerate belts. It can be seen that the second component makes a dominant contribution. A comparison group of the EEMD energy ratios of ten different potholes is plotted in Figure 5(b), which suggests that the first and second components have comparable weight in some cases.

Finally, energy entropy is proposed to describe the different energy distributions with $H = -\sum_{k=1}^{N} E_k \cdot \log E_k$. For a decelerating belt being pressed on both tires, its vibration focuses on only several frequencies, with less energy uncertainty and smaller energy entropy than a pothole. Therefore, decelerating belts can be removed when the energy entropy is less than a predefined threshold T_h.

4.7 Data fusion

After pothole extraction, the central server gathers multiple vehicles' pothole detection results. Next, it counts reports of each potential potholes. Finally, it declares a pothole when the report count is larger than a threshold P; otherwise, it marks these pothole detection results as false alarms.

5 Road surface roughness classification

In this section we describe an online data mining algorithm to classify road surface roughness into four levels.

5.1 Distributed road roughness classification

5.1.1 International roughness index

International Roughness Index (IRI) is the most widely used metric for evaluating road roughness in highway transportation. According to the highway safety research institute, IRI is defined as the responses of the quarter car model [8,20]. It reflects the global vibration of the road, which can be measured by an accelerometer.

Lou el al. [16] show that the empirical relationship between IRI and standard deviation of vibration σ can be approximated by the following regression equation:

$$IRI = \frac{\sigma - 0.013}{0.5926}, \tag{14}$$

where σ is the standard deviation of the continuous accelerometer from road vibration.

The relationship between the standard deviation and the expectation can be described as follows:

$$\sigma^2 = E^2[x(t)] + E[x^2(t)], \tag{15}$$

where $E[x(t)]$ represents the expectation of the continuous accelerometer $x(t)$.

5.1.2 Road roughness level classification

The technical Code of Maintenance for Urban Road CJJ36-2006 [25] is an industry standard in China. This industry standard indicates that road roughness levels can be evaluated by a comprehensive comfortable driving metric, Riding Quality Index (RQI).

Generally, road roughness is classified into four levels, namely, excellent, good, qualified, and unqualified, with different RQIs and driving velocities. These evaluation standards for pavement roughness are listed in Table 1.

Yang [25] shows that the relationship between RQI and IRI can be described mathematically as:

$$RQI = 4.98 - 0.34 \cdot IRI. \tag{16}$$

Additionally, the numerical value of RQIs normally vary from 0 to 5. We set RQI to 0 when it is negative.

In the CRSM system, the onboard hardware devices collect acceleration readings, calculate the standard deviation σ and IRI, classify road roughness into these above four levels, and periodically transmit recent road roughness levels to the central server.

Table 1: Evaluation standards of road roughness levels.

v(km/h)	RQI	Pavement roughness level
v>80	RQI>3.6	excellent
	3.0<RQI<3.6	good
	2.5<RQI<3.0	qualified
	0<RQI<2.5	unqualified
40<v<80	RQI>3.2	excellent
	2.8<RQI<3.2	good
	2.4<RQI<2.8	qualified
	0<RQI<2.4	unqualified
v<40	RQI>3.0	excellent
	2.6<RQI<3.0	good
	2.2<RQI<2.6	qualified
	0<RQI<2.2	unqualified

5.2 Central server data fusion

The central server collects reports from these distributed CRSM hardware devices, and then makes a comprehensive evaluation of road roughness levels of different road sections in a city region.

6 Evaluation

This section presents field test results of the CRSM system and discuss its performance in different aspects.

6.1 Environments and Methodology

Our experiments were primarily conducted in the Shenzhen urban area. We selected 100 taxies and equipped each of them with a CRSM device. To obtain ground truth for our experiments, we used a camera to record road surface videos for comparison. We also tested our system on a car in Highway Traffic Testing Field of Ministry of Transportation in Beijing, which is a national traffic testing environment in China. Unless stated explicitly, the results discussed in this section are with the first scenario.

The CRSM module is attached to the right side of the dashboard to sense the vibration. We need to place the three-axis accelerometer in a particular direction, where its x-axis is kept in the same direction as the driving direction, its y-axis in the corresponding horizontal direction, and the its z-axis is in the vertical direction. In practice, a GPS receiver often fails to work in urban canyons with tall buildings and tunnels, which leads to missed GPS data. Also, a GPS receiver normally needs around 40 seconds to obtain the first fix after being powered on, during which time the produced positions

may be wrong. Transmission errors can also cause temporary data outage.

To solve these problems, we propose an effective data cleaning algorithm. We first sort the raw data in a time sequence, detect GPS bad zones with large amounts of data missing or discontinuity, and remove these bad zones directly. Then, we check transmission errors and short GPS missing, and record the time indexes. Next, we generate interpolated points in curves to get continuous data. Finally, our data cleaning algorithm results are organized as elements in the form: <time, location, velocity, three-axis acceleration>. [1]

6.2 Road pothole detection

6.2.1 i-GMM based event detection

There are several thresholds to be determined in the i-GMM. As we cannot reduce false alarms and data missing rate at the same time, there is always a trade-off between them. In CRSM, we would like to keep the information of potential potholes, even with some false alarms. Actually, most false alarms can be removed by pothole filters and data fusion in the central server. We keep the missed event rate below 5% with the following threshold setting: (i) Z-peak parameters: two different thresholds $Z_{th1} = 1$, and $Z_{th2} = 2.2$. (ii) GMM parameters: Gaussian number $K = 4$, initial Gaussian mean $\mu_0 = 0$, variance $\sigma_0 = 10$, weight $\omega_0 = 0.15$, sum of most likely distribution weight $T = 0.7$. (iii) i-GMM parameters: maximum and minimum of learning rate $\alpha_{max} = 0.04$, $\alpha_{min} = 0.02$, event detection threshold $M_{th} = 0.25$, two different velocity thresholds $V_{th} = 50$, and $V_{tc} = 15$.

Figure 6 shows the comparison of the Z-peak, GMM event detection and the i-GMM event detection. Figures 6(a) and 6(b) are the z-axis acceleration and velocity, respectively. Figures 6(c) and 6(d) are the event detection results of Z-peak with threshold $Z_{th} = 1$, Z-peak with threshold $Z_{th} = 2.2$, while Figures 6(e) and 6(f) are event detection results of the GMM and the i-GMM, where each vertical line indicates an effect event.

We can see that Z-peak reports many events with a low threshold, and fewer events with a high threshold. It means that Z-peak is very dependent on current vibrations and predefined parameters, which are unable to be updated with online learning. As can be seen from

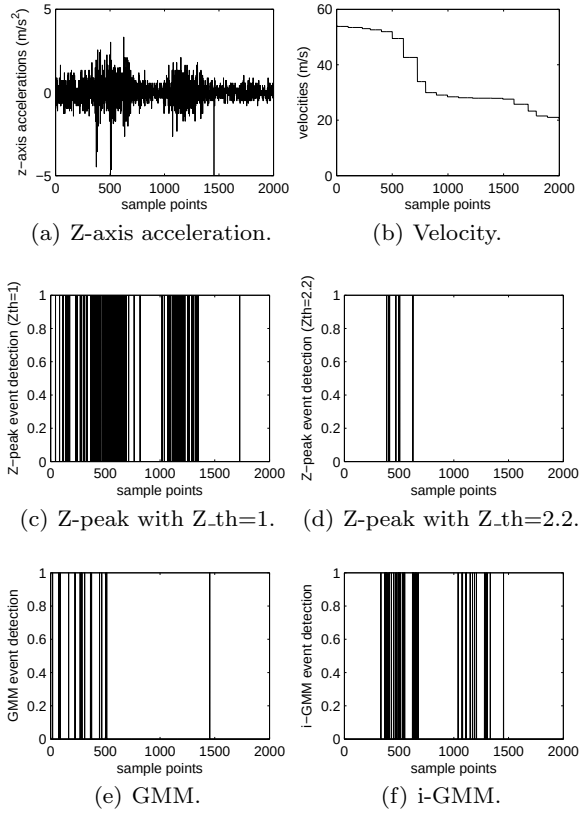

(a) Z-axis acceleration. (b) Velocity.

(c) Z-peak with Z_th=1. (d) Z-peak with Z_th=2.2.

(e) GMM. (f) i-GMM.

Fig. 6: Comparison of event detection results.

Figure 6(e), the GMM behaves well with online learning progress, even with naive initial Gaussian parameters. However, the GMM still has many false alarms for a high velocity, with missing events at a small velocity, while the i-GMM can solve this problem.

6.2.2 Pothole detection with four filters

The central server applies four pothole filters to remove irrelevant events, and combines multiple vehicles' pothole detection results. Table 2 lists pothole events and several disturbance events, as well as their occurrence counts. Four potholes filters are used to remove these spurious events later. Table 3 lists the true positive (TP) and false positive (FP) of each filter. Figure 7 shows the cumulative density function (CDF) that describes the feature of each filter.

Figure 7(a) presents the CDF of the velocity filter, which removes events with small velocities. For $T_V = 16.3$, it rejects all low velocity events with nearly 87.1% pothole detection accuracy and zero false alarms. Figure 7(b) shows the CDF of the z-axis acceleration filter, which discards events with small z-axis accelerations like those from small bumps. With $T_Z = 1.82$, it achieves 87.1% pothole detection accuracy with 8.07%

[1] There are various ways to deal with the problem of GPS signal being temporarily unavailable. For example, the Siemens car navigation system uses Kalman filters and auxilliary sensors [17] for dead reckoning. To simplify the online data mining algorithm, we have used a simple interpolation method, instead of more sophisticated methods.

Table 2: Reported numbers of various events.

Event types	Occurrences
Potholes	170
Low velocity events	133
Small bumps	51
Expansions	58
High velocity events	38

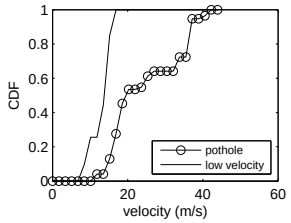

(a) Velocity filter.

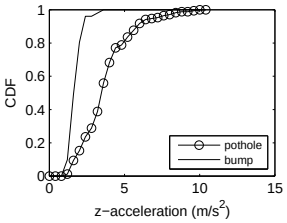

(b) Z-axis acceleration filter.

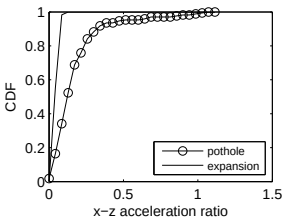

(c) X-z acceleration ratio filter.

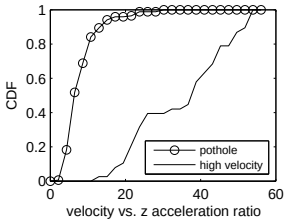

(d) Velocity vs. z-axis acceleration ratio filter.

Fig. 7: CDF of four pothole filters.

of false alarms. Figure 7(c) describes the CDF of the x-z acceleration ratio filter, which removes events with a small ratio of x-axis acceleration to z-axis acceleration. With $T_{XZ} = 0.05$, it acquires 82.4% pothole detection accuracy with 7.89% of false alarms. Figure 7(d) presents the CDF of the velocity vs. z-axis acceleration ratio filter, which removes events with high velocity vibration. With $T_{VZ} = 16$, it obtains 94.7% pothole detection accuracy with 0.62% false alarms.

With distributed vehicle data fusion, we can further reduce false alarms which appear rarely in other vehicles. In general, the CRSM system can achieve as high as 90% pothole detection accuracy, with nearly zero false alarms.

6.2.3 EEMD based pothole extraction

The central sever utilizes an EEMD-based pothole extraction method to reject decelerating belts. The collected accelerations are first decomposed with a fast EEMD tool [22], and the energy entropies are determined with the most significant four energy components, as shown in Figure 8. With a energy entropy threshold $T_e = 0.95$, decelerating belts are removed with 85% accuracy.

Table 3: The true positive (TP) and false positive (FP) of each filter.

Filters	TP	FP
Velocity filter	148	0
Z-acceleration filter	148	13
X-z ratio filter	140	12
Velocity vs. z ratio filter	161	1

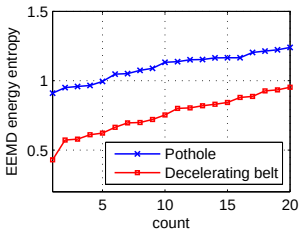

Fig. 8: EEMD energy entropy of potholes and decelerating belts.

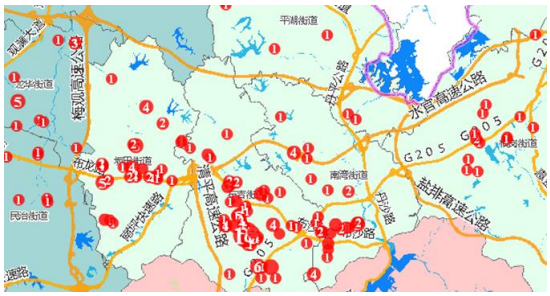

Fig. 9: Pothole map in the Longgang District, Shenzhen.

6.2.4 Final results

Based on the i-GMM based event detection algorithm, each CRSM device transfers less than 15 MB data to the center server monthly. The central server gathers pothole locations and counts from different vehicles. After processing, the potholes are plotted in GoogleMap with GPS locations. Here, the ArcGis [2] engine APIs are used for geographic information processing.

Figure 9 shows a real pothole map in the Longgang district of Shenzhen, where red circles represent road potholes. For a better display, we use a density-based clustering method to group nearby potholes, where the group size is shown in the center of the red circle. For example, a red circle with number five means that there are five potholes near this location.

We also run our system on a car in the Highway Traffic Testing Field of Ministry of Transportation in

(a) A perspective view.

(b) Road with stone blocks.

(c) Gravel road.

Fig. 10: Highway Traffic Testing Field of Ministry of Transportation in Beijing.

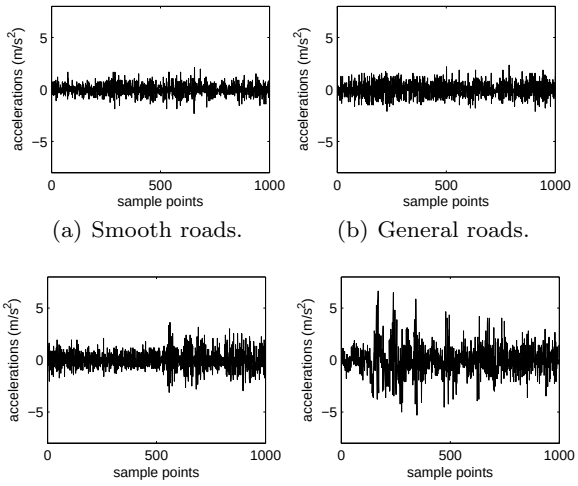

(a) Smooth roads. (b) General roads.

(c) Roads with bumps. (d) Roads with potholes.

Fig. 11: Continuous z-axis accelerations of different road types.

Beijing. Figure 10 shows the perspective view and two typical roads, namely stone block roads and washboard roads, in this national traffic testing environment in China. The vehicle equipped with a CRSM devices traveled on a 18km long road with many potholes, cobblestones, ripples, stones, vehicle braking, high velocity driving, turnings, and decelerating belts. In this trace, CRSM detected 49 road potholes accurately, without any false alarm. It is important to note that we used only a single vehicle in this field (due to restriction of field usage and cost), which led to 9 potholes being missed. We expect that when multiple vehicles are available, CRSM can further reduce the error rate with our data fusion technique.

6.3 Road roughness level classification

We collect acceleration data from actual roads with different characteristics: (I) smooth and clean roads with little sand and gravel, (II) general roads with some sand or small stones, (III) roads with small bumps, (IV) roads with potholes.

Figure 11 shows the continuous z-axis accelerations against sampling points on various types of roads, where (a) to (d) stand for smooth roads, general roads, roads with bumps, and roads with potholes, respectively.

As shown in Figure 11(a), the z-axis accelerations on smooth roads are very regular, with only small fluctuations in the middle. From Figure 11(b), we can see that there are relatively larger amplitudes in the z-axis accelerations on general roads than on smooth roads. It might be caused by disturbances from small sand or small stones on the road surface, though the overall road condition is very good. Figure 11(c) presents the z-accelerations on roads with bumps. We find some larger fluctuations due to several small bumps. This road is also considered to be qualified in spite of these disturbances. Figure 11(d) shows the z-axis accelerations data on roads with potholes. The acceleration data are with great fluctuations, and we conclude that the vehicles experience strong vibrations when passing these potholes. The road condition is therefore unqualified in general.

Distributed onboard modules transmit road roughness levels to the central sever periodically. Then road roughness is evaluated into levels with maximum report times in our central server. Road roughness levels of various road types are listed in Table 4. These four road types with different velocities are classified into levels of excellent, good, qualified, and unqualified, which are in conformity with the above discussion.

Experimental results show that the CRSM can evaluate road roughness levels correctly, even with some interference from small bumps or potholes. Furthermore, the CRSM onboard module consumes no more than 50 dollars in total, which is only 1/4400 to 1/160 of these existing systems [4] with a cost of about $8,000-222,000$. Therefore, CRSM is more affordable, and more likely to be widely adopted in municipal engineering.

Table 4: Road roughness levels of various road conditions.

Road type	Velocity	RQI	Road roughness level
Smooth	37.15	3.52	excellent
General	63.86	3.12	good
Bumps	62.36	2.66	qualified
Potholes	37.50	1.14	unqualified

7 Future work

There are two types of events, decelerating belt, which causes vibrations similar to those by potholes. We have tried different algorithms to analyze the data in both time and frequency domains, and found it is still difficult to draw a clear distinction. In our system, a single decelerating belt can be filtered out with EEMD energy ratio. However, manholes and continuous decelerating belts generate similar vehicle vibrations as potholes, so it is hard to identify them simply with acceleration information. In CRSM, we discover the geographic locations of manholes and decelerating belts from the urban traffic database, and remove these two types of events with their GPS information. However, this method does not apply to village roads, which may not have the desired information registered. We thus need to explore more effective methods in our future work.

Furthermore, vibration signals vary greatly with many factors such as vehicles' loads, driving velocities, and drivers' habits. We will also study these factors and establish a comprehensive model in our future work.

8 Conclusion

In this paper, we have described the design and implementation of CRSM, a crowdsourcing-based road surface monitoring system. It can monitor road potholes and road roughness levels simultaneously, with distributed modules mounted on vehicles. Experimental results show that CRSM can detect road potholes with up to 90% accuracy, and nearly zero false alarms. CRSM can also evaluate road roughness levels accurately, even with some interferences from small bumps or potholes.

Acknowledgements Kongyang Chen's work was supported in part by the SIAT Innovation Program for Excellent Young Researchers (201307). Guang Tan's work was supported by the National Science Foundation of China (NSFC) under Grants 61103243 and 61379135. Mingming Lu's work was supported in part by the NSFC under grant 60903222. Jie Wu's work was supported in part by US NSF grants ECCS 1231461, ECCS 1128209, CNS 1138963, CNS 1065444, and CCF 1028167.

References

1. ABCChicago. Find a claim, reporting a pothole. http://abc7chicago.com/archive/5942405/.
2. ArcGIS. http://en.wikipedia.org/wiki/ArcGIS_Explorer.
3. U.S. Federal Highway Administration. 2010 status of the nation's highways, bridges, and transit: conditions & performance. http://www.fhwa.dot.gov/policy/2010cpr/index.htm.
4. A synopsis on the current equipment used for measuring pavement smoothness. http://www.fhwa.dot.gov/pavement/smoothness/rough.cfm.
5. Basharat, A., Gritai, A., & Shah, M. (2008). Learning object motion patterns for anomaly detection and improved object detection. In *Proceedings of IEEE Conference on Computer Vision and Pattern Recognition (CVPR)*.
6. Chen, K., Lu, M., Tan, G., & Wu, J. (2013). CRSM: Crowdsourcing based Road Surface Monitoring. In *Proceedings of IEEE/IFIP International Conference on Embedded and Ubiquitous Computing*.
7. Christian, K., & Ioannis, B. (2011). Pothole detection in asphalt pavement images. *Advanced Engineering Informatics*, 25, 507-515.
8. Dodds, C., & Robson, J. (1973). The description of road surface roughness. *Journal of Sound and Vibration*, 31, 175-183.
9. Dyer, J., Dyer, D., & Devore, J. (2009). Estimating International Roughness Index from noisy profilograph measurements. In *Proceedings of IEEE Instrumentation and Measurement Technology Conference*.
10. Eriksson, J., Girod, L., & Hull, B. (2008). The Pothole Patrol: using a mobile sensor network for road surface monitoring. In *Proceedings of International Conference on Mobile Systems, Applications, and Services (MobiSys)*.
11. Hou, Z., Wang, K., & Gong, W. (2007). Experimentation of 3D pavement imaging through stereovision. In *Proceedings of International Conference on Transportation Engineering*.
12. Jason, M., Claire, S., Stephen, M., & Denis, T. (2012). 3D laser imaging for surface roughness analysis. In *International Journal of Rock Mechanics and Mining Sciences*, 58, 111-117.
13. Kasun, Z., Chamath, K., Gihan, S., & Shihan, W. (2007). A public transport system based sensor network for road surface condition monitoring. In *Proceedings of the 2007 workshop on Networked systems for developing regions*.
14. Li, Q., Yao, M., Yao, X., & Xu, B. (2010). A real-time 3D scanning system for pavement distortion inspection. *Measurement Science and Technology*, 21(1), 15702-15709.
15. Lin, H., Chuang, J., & Liu, T. (2011). Regularized Background Adaptation: A Novel Learning Rate Control Scheme for Gaussian Mixture Modeling. *IEEE Transactions on Image Processing*, 20, 822-836.
16. Lou, S., Wang, Y., & Xu, C. (2007). Study of calculation of IRI based on power spectral density of pavement surface roughness. *Journal of Highway and Transportation Research and Development*, 24, 12-15.
17. Mandic, D., Golz, M., Kuh, A., Obradovic, D., & Tanaka, T. (2008). Signal Processing Techniques for Knowledge Extraction and Information Fusion. *Springer Press*.
18. Mohannad, M., Marwan, S., & Isam, S. (2012). Numerical modeling of traffic-induced ground vibration. *Computers and Geotechnics*, 39, 116-123.
19. Prashanth, M., Venkata, N., & Ramachandran, R. (2008). Nericell: Rich monitoring of road and traffic conditions

using mobile smartphones. In *Proceedings of International Conference on Embedded Networked Sensor Systems (Sensys)*.

20. Semiha T., & Huseyin, A. (2005). A study of random vibration characteristics of the quarter-car model. *Journal of Sound and Vibration*, 282, 111-124.
21. Tan, G., Lu, M., Jiang, F., Chen, K., Huang, X., & Wu, J. (2014). Bumping: A Bump-Aided Inertial Navigation Method for Indoor Vehicles Using Smartphones. *IEEE Transactions on Parallel and Distributed Systems*, 25(7), 1670-1680.
22. Wang, Y., Yeh, C., Young, H., Hu, K., & Lo, M. (2014). On the computational complexity of the empirical mode decomposition algorithm. Physica A: Statistical Mechanics and its Applications, 400(15), 159-167.
23. Wu, Z., & Huang, N. (2009). Ensemble empirical mode decomposition: a noise-assisted data analysis method. *Advances in Adaptive Data Analysis*, 1, 1-41.
24. Xu, D., Mohamed, A., Yong, R., & Caporuscio, F. (1992). Development of a criterion for road surface roughness based on power spectral density function. *Journal of Terramechanics*. 29, 477-486.
25. Yang, S. (2006) Technical Code of Maintenance for Urban Road CJJ36-2006. *China Architecture and Building Press*.
26. Yu, B., & Yu, X. (2006). Vibration-based system for pavement condition evaluation. In *Proceedings of International Conference on Applications of Advanced Technology in Transportation*.
27. Yu, X., & Salari, E. (2011). Pavement pothole detection and severity measurement using laser imaging. In *Proceedings of IEEE International Conference on Electro/Information Technology*.
28. Zhang, Y. & Ma, R. (2009). A study of pavement roughness measurement system based on laser ranger finder. In *Proceedings of International Conference on Image Analysis and Signal Processing*.

Kongyang Chen received the B.S. and M.E. degrees from Central South University, China. After that, he joined the Shenzhen Institutes of Advanced Technology, Chinese Academy of Sciences, China. He is currently working toward the PhD degree in the Shenzhen College of Advanced Technology, University of Chinese Academy of Sciences. His research interests include wireless sensor network and mobile sensing.

Guang Tan is currently an Associate Professor at Shenzhen Institutes of Advanced Technology (SIAT), Chinese Academy of Sciences, China, where he works on the design of distributed systems and networks. He received his PhD degree in computer science from the University of Warwick, U.K., in 2007. From 2007 to 2010 he was a postdoctoral researcher at INRIA-Rennes, France. He has published more than 30 research articles in the areas of peer-to-peer computing, wireless sensor networks, and mobile computing. His research is sponsored by National Science Foundation of China and Chinese Academy of Sciences. He is a member of IEEE, ACM, and CCF.

Mingming Lu is an Associate Professor of Central South University (CSU). Before he joined CSU, he worked for Citrix System Inc. Mingming Lu got his PhD in Computer Science from Florida Atlantic University, USA in 2008. He got his master and bachelor degrees from Fudan University and Tongji University in 2003, and 2000, respectively. His research areas include opportunistic sensing, compressive sensing, routing algorithm, network coding, localization, and wireless/mobile sensor networks, etc. He has published over 30 scholarly journal and conference papers. He was a TPC member of IEEE INFOCOM 2011 and reviewers of numerous international journals and conference such as TPDS, TMC, ICNP, MobiHoc etc.

Jie Wu is Chair and Laura H. Carnell Professor in the Department of Computer and Information Sciences at Temple University. He was a program director at the National Science Foundation and Distinguished Professor at Florida Atlantic University. His research interests include wireless networks, mobile computing, routing protocols, fault-tolerant computing, and interconnection networks. Dr.Wus publications include over 600

papers in scholarly journals, conference proceedings, and books. He has served on several editorial boards, including IEEE Transactions on Computers and Journal of Parallel and Distributed Computing. Dr. Wu was general co-chair for IEEE MASS 2006, IEEE IPDPS 2008, and IEEE DCOSS 2009 and was the program co-chair for IEEE INFOCOM 2011. He served as general chair for IEEE ICDCS 2013. He was an IEEE Computer Society Distinguished Visitor and the chair for the IEEE Technical Committee on Distributed Processing (TCDP). Currently, Dr. Wu is an ACM Distinguished Speaker and a Fellow of the IEEE. He is the recipient of 2011 CCF Overseas Outstanding Achievement Award.